Low-frequency SST and upper-ocean heat content variability in the North Atlantic

Martha W. Buckley and Rui M. Ponte (Atmospheric and Environmental Research) and Gaël Forget (Massachusetts Institute of Technology)

Motivation

- **Observations indicate Atlantic SSTs exhibit significant low-frequency variability** (Bjerknes 1964; Kushnir 1994; Ting et al. 2009).
  - e.g. Atlantic Multidecadal Oscillation (Kerr, 2000; Knight et al., 2005)
- **The origin of Atlantic SST anomalies is not known.**
- Likely depends on **timescale**
  - Intra-annual to inter-annual: response to local atmospheric forcing (Frankignoul and Hasselmann, 1977), e.g. the NAO tripole (Cayan, 1992).
  - Longer timescales (how long?) ocean circulation may play a role.
- **Ocean dynamics that are important have not been isolated**
  - Wind and/or buoyancy forced baroclinic Rossby waves (Sturges et al 1998).
  - Large scale changes in Atlantic ocean heat transport due to changes in the AMOC (Kushnir 1994, etc.) and gyre circulations.
  - Lozier (2010): most significant question concerning the AMOC is role of AMOC in creating decadal SST anomalies.

Question

What are the relative roles of atmospheric forcing and ocean dynamics in setting upper-ocean heat content variability in the North Atlantic?

ECCO version 4 state estimate (1992-2010)

- MITgcm least squares fit to observations using adjoint (Wunsch et al., 2009)
- fit achieved by adjusting initial conditions, forcing, and model parameters
- well-suited to understand UOHC variability because it satisfies equations of motion and preserves property budgets exactly (Wunsch and Heimbach, in press).
- Atmospheric forcing: ERA-Interim
- Ocean data:
  - In-situ: Argo, CTDs, XBTs, mooring arrays
  - Satellite: AVHRR & AMSR-E SST, altimetry
- Model Details (G. Forget)
  - New global grid (LLC90): includes Arctic, 50 vertical levels with partial cells
  - Nominal 1° resolution with telescopic resolution to 1/3° near Equator
  - State of the art dynamic/thermodynamics sea ice model
  - Nonlinear free surface + real freshwater fluxes

Comparison to observations

Temperature Misfits

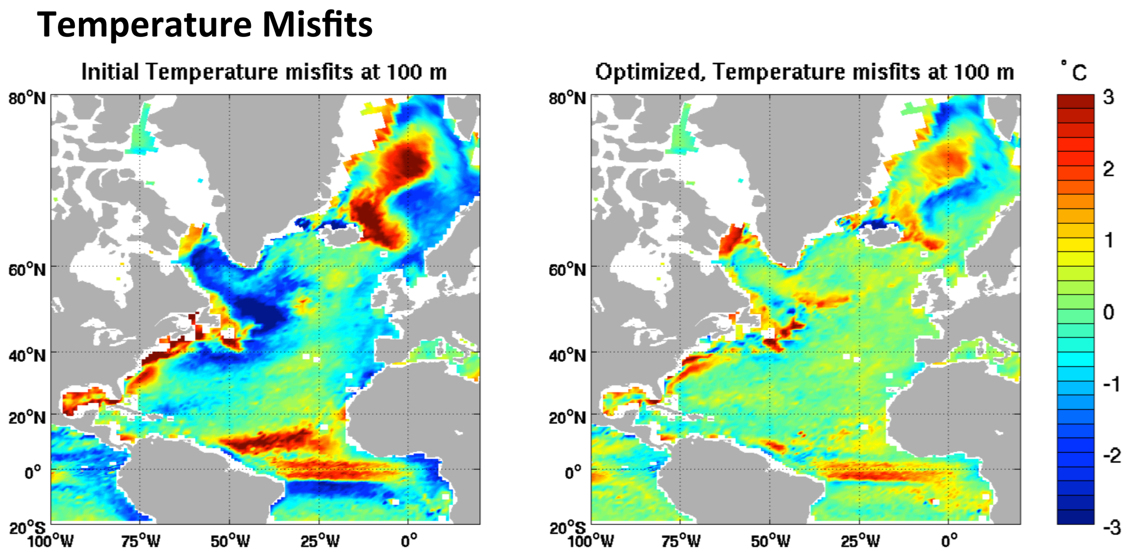

Temperature misfits for (left) "first-guess" solution and (right) optimized ECCO v4 solution at 100 m depth for all in-situ data (Argo, CTDs, XBTs, SeaOs) averaged over 1992-2010. Misfits are calculated as the sample mean for each grid cell of $T_e - T_o$, where T_o are observational profiles and T_e are the corresponding profiles from the model.

Comparison of observed and ECCO v4 SST variability

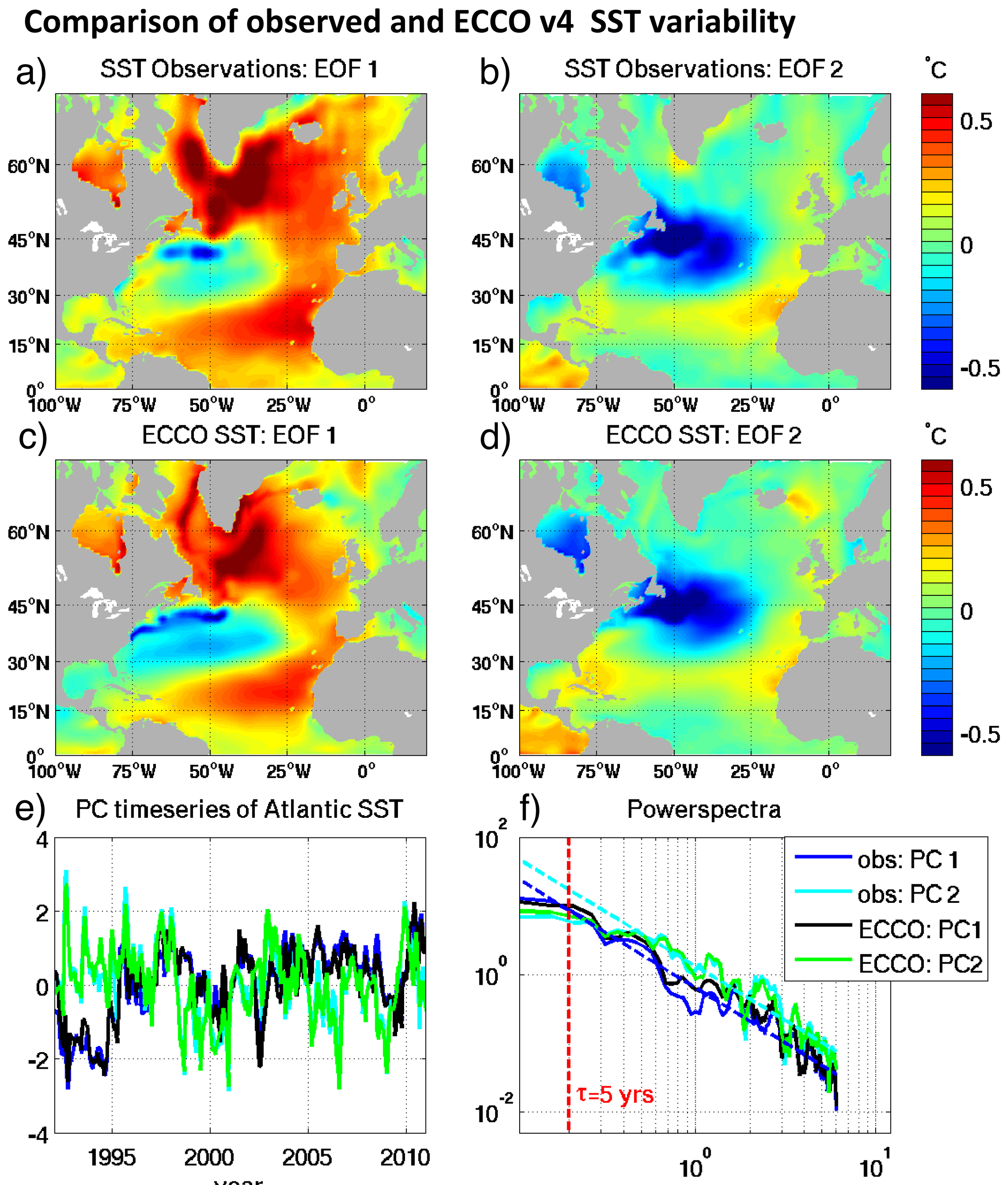

The first two empirical orthogonal functions (EOFs) of monthly (seasonal cycle removed) North Atlantic SST anomalies from (a-b) mapped Reynolds et al. (2002) data and (c-d) ECCO v4, which respectively explain ~25% and ~15% of the spatially integrated variance. (e) The first two principal component (PC) time series and (f) respective power spectra.

Upper-ocean heat content variability

Heat Content integrated over maximum climatological mixed layer depth (D)

- Measure of heat contained in "active" ocean layers
- Implicitly accounts for reemergence of SST anomalies (Deser et al, 2003; Coetlogon and Frankignoul, 2003; Buckley et al, subm.)
- Define: $H = \rho_o C_p \int_{-D}^{\eta} T\, dz$

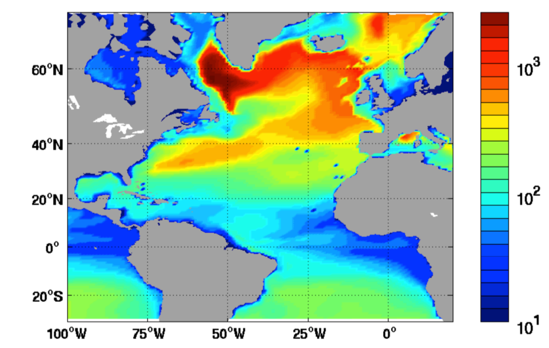

Maximum Climatological mixed layer depth (D)

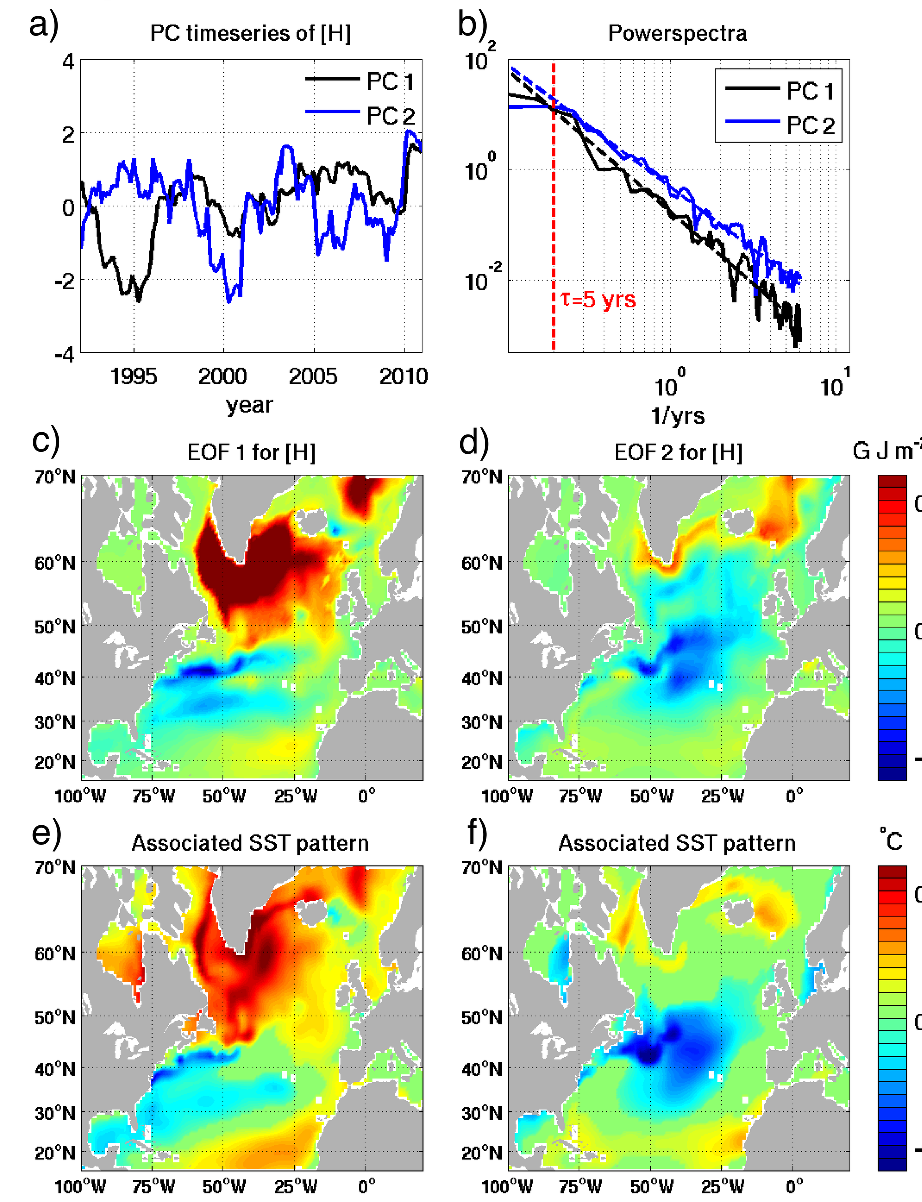

To right:
(a) The first two PC time series of monthly H anomalies (seasonal cycle removed) over the North Atlantic and (b) their respective power spectra.
(c-d) The first two EOFs of North Atlantic H.
(e-f) The spatial patterns of SST variability associated with the first two PC time series of North Atlantic H, obtained by projecting the PC time series onto monthly SST anomalies (seasonal cycle removed).

Heat content budgets

$$\underbrace{\rho_o C_p \int_{-D}^{\eta} \overline{\frac{\partial T}{\partial t}}\, dz}_{H_t} = \underbrace{-\rho_o C_p \int_{-D}^{\eta} \nabla\cdot(\overline{\mathbf{u}T}+\overline{\mathbf{u}^* T})\, dz}_{C_{adv}} - \underbrace{\rho_o C_p \int_{-D}^{\eta} \overline{\nabla\cdot\mathbf{K}}\, dz}_{C_{diff}} + \overline{Q}_{net}$$

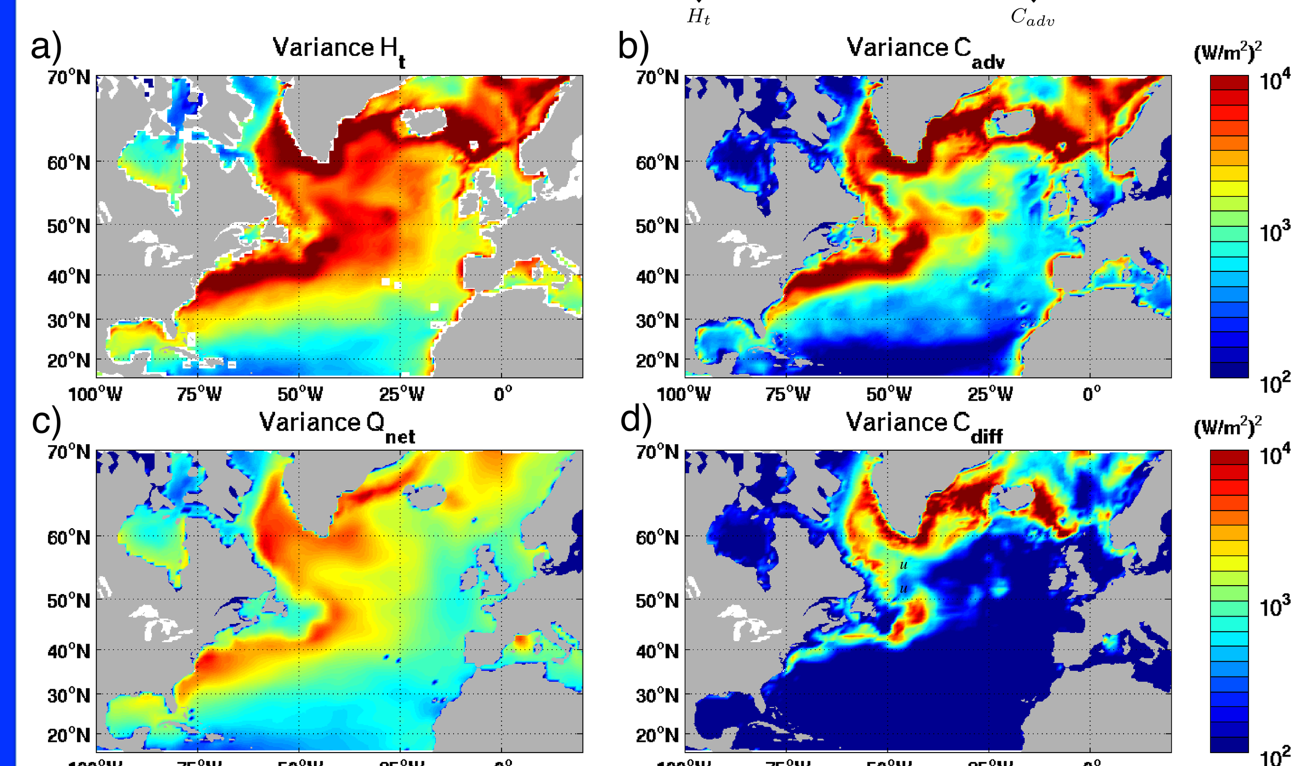

Variance of monthly anomalies (seasonal cycle removed) of terms in the H_t budget. (a) tendency H_t, (b) advective convergence C_{adv}, (c) air-sea heat flux Q_{net} and (d) diffusive convergence C_{diff}.

Advective convergences play a large role in H_t budget in areas of strong currents/fronts, such as along the Gulf Stream path.

Dynamics of Advective heat transport convergences

$$\mathbf{u_g} = \frac{1}{f\rho_o}\hat{\mathbf{z}}\times\nabla p, \quad \mathbf{u_{ek}} = \frac{\tau\times\hat{\mathbf{z}}}{\rho_o f D_{ek}}, \; D_{ek} = \min(D, 100\text{ m})$$

$$w(-D) \approx \int_{-D}^{\eta}\nabla_H\cdot\mathbf{u}\, dz \approx \underbrace{\int_{-D_{ek}}^{\eta}\nabla_H\cdot\mathbf{u_{ek}}\, dz}_{\equiv w_{ek}(-D)} + \underbrace{\int_{-D}^{\eta}\nabla_H\cdot\mathbf{u_g}\, dz}_{\equiv w_g(-D)}$$

$$C_{adv} = \underbrace{-\rho_o C_p \int_{-D}^{\eta}\nabla\cdot(\bar{\mathbf{u}}\bar{T})\, dz}_{\text{linear: } C_{lin}} \underbrace{-\rho_o C_p \int_{-D}^{\eta}\nabla\cdot(\overline{\mathbf{u}'T'}+\overline{\mathbf{u}^*T})\, dz}_{\text{bolus: } C_{bol}}$$

$$C_{ek} = \rho_o C_p \int_{-D_{ek}}^{\eta}\nabla\cdot(\bar{\mathbf{u}}_{\mathbf{ek}}\bar{T})\, dz + \rho_o C_p\, \overline{w}_{ek}(-D)\, \overline{T}(-D)$$

$$C_g = \rho_o C_p \int_{-D}^{\eta}\nabla\cdot(\bar{\mathbf{u}}_{\mathbf{g}}\bar{T})\, dz + \rho_o C_p\, \overline{w}_g(-D)\, \overline{T}(-D)$$

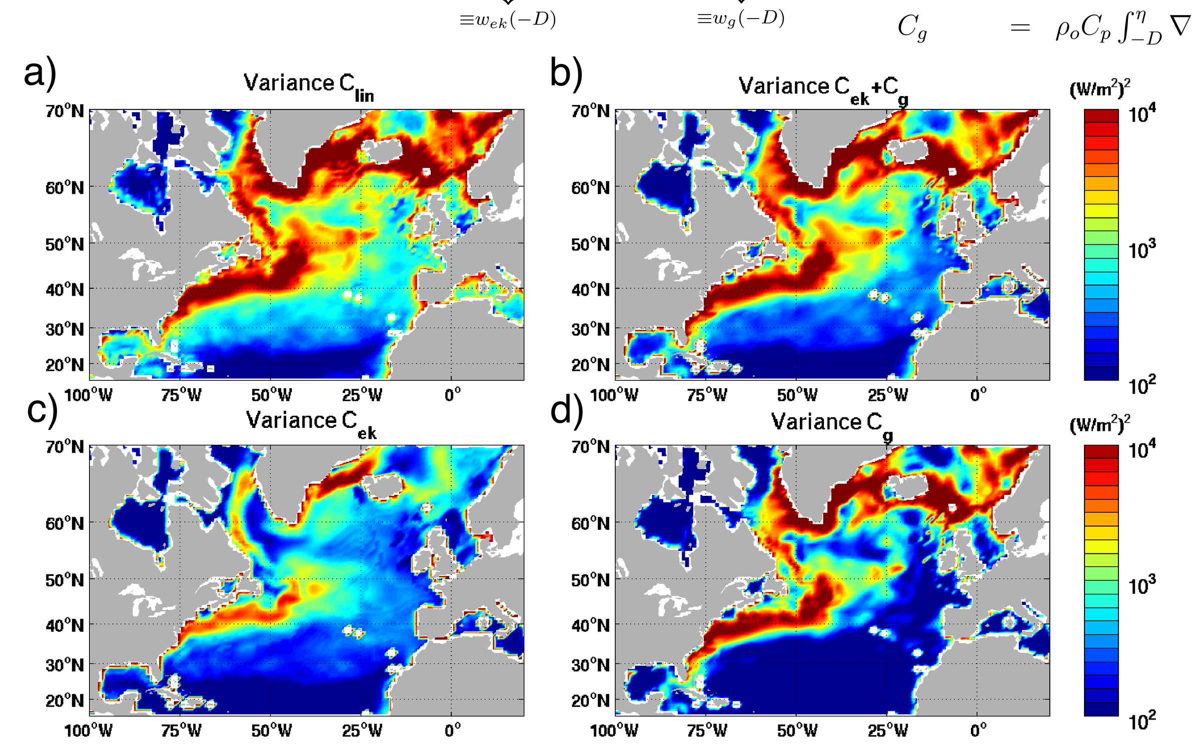

Notation:

- ū, etc. are monthly means
- u' etc. are deviations from monthly means
- u* is the eddy induced transport velocity parameterized by the Gent and McWilliams (1990) scheme.

- Variance of C_{lin} and $C_{ek}+C_g$ similar to that of C_{adv} in most regions.
- Both C_{ek} and C_g are largest in regions of strong currents/ fronts.
- C_{ek} also plays a role in gyre interiors.

Variance of monthly anomalies of components of advective convergence C_{adv}, a) linear C_{lin}, b) estimated $C_{ek}+C_g$, c) Ekman C_{ek}, and d) geostrophic C_g.

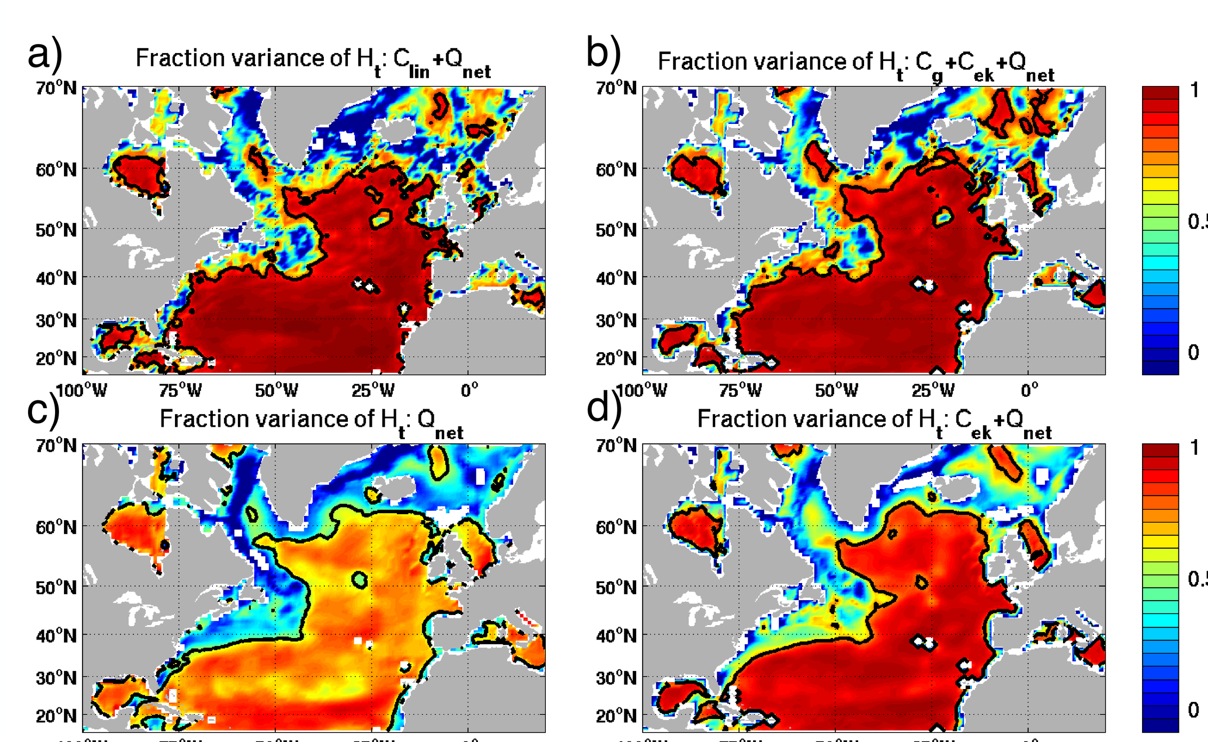

- Variance of H_t is well explained by $Q_{net}+C_{lin}$ or $Q_{net}+C_{ek}+C_g$ in most regions. Exceptions:
  - Mann Eddy region
  - shallow subpolar regions
- In gyre interiors
  - About 50% of variance of H_t explained by Q_{net}.
  - More than 70% of variance of H_t explained by local forcing $C_{loc}=C_{ek}+Q_{net}$.
- Geostrophic convergences important along Gulf Stream path

Maps showing the fraction of the variance of H_t explained by a) $C_{lin}+Q_{net}$ b) $C_{ek}+C_g+Q_{net}$, c) Q_{net}, and d) $C_{loc}=C_{ek}+Q_{net}$. Black contours are where the fraction of the variance is 0.7.

Regionally integrated budgets

Fluxes: terms in regionally integrated budgets

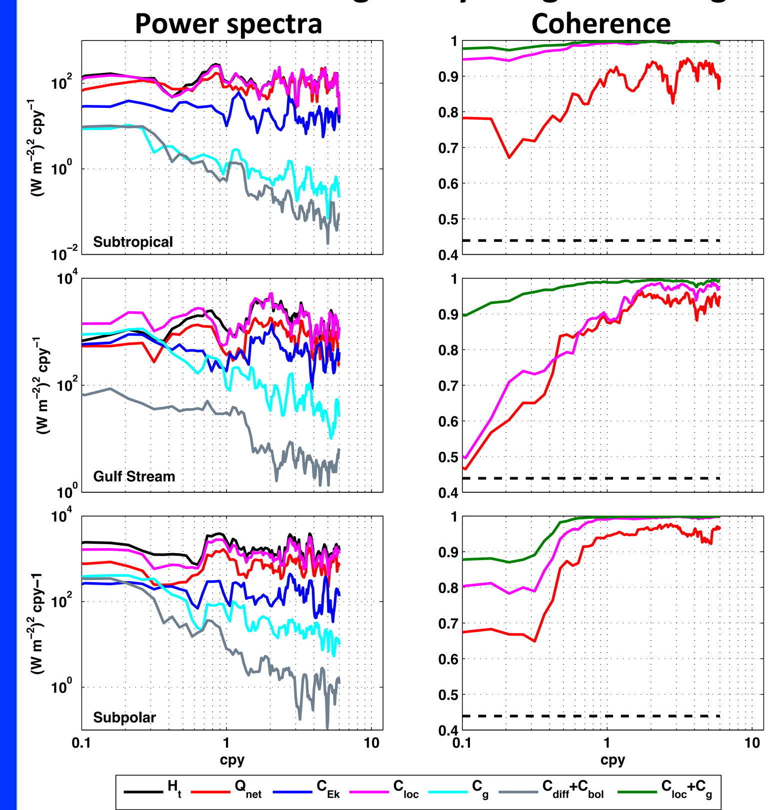

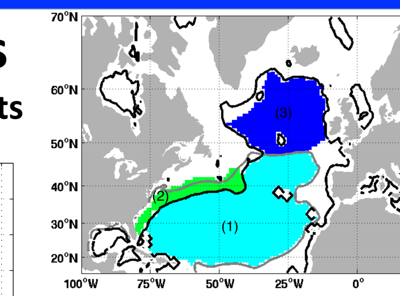

Regions: (1) subtropical gyre interior, (2) Gulf Stream region, and (3) subpolar gyre interior.

1) Subtropical gyre
   - ➢ C_{loc} dominates for all τ
2) Gulf Stream
   - ➢ C_{loc} dominates for τ<6 mo
   - ➢ C_g has increasing role for τ>6 mo
3) Subpolar gyre
   - ➢ C_{loc} dominates for τ< 1 yr
   - ➢ C_g, C_{diff}, C_{bol} all play a role for τ> 1 yr.

(left panels) Power spectra of terms in H_t budget and (right panels) magnitude squared coherence between H_t and Q_{net}, C_{loc}, and $C_{loc}+C_g$ for (top panels) subtropical gyre (middle panels) Gulf Stream region and (bottom panels) subpolar gyre.

Temporally integrated regional budgets

$$\underbrace{\int_0^t \frac{H_t}{\rho_o C_p V}\, dt}_{\equiv(T-T_o)} = \underbrace{\int_0^t \frac{C_{adv}}{\rho_o C_p V}\, dt}_{\equiv T_{adv}} + \underbrace{\int_0^t \frac{C_{diff}}{\rho_o C_p V}\, dt}_{\equiv T_{diff}} + \underbrace{\int_0^t \frac{Q_{net}}{\rho_o C_p V}\, dt}_{\equiv T_{air-sea}}.$$

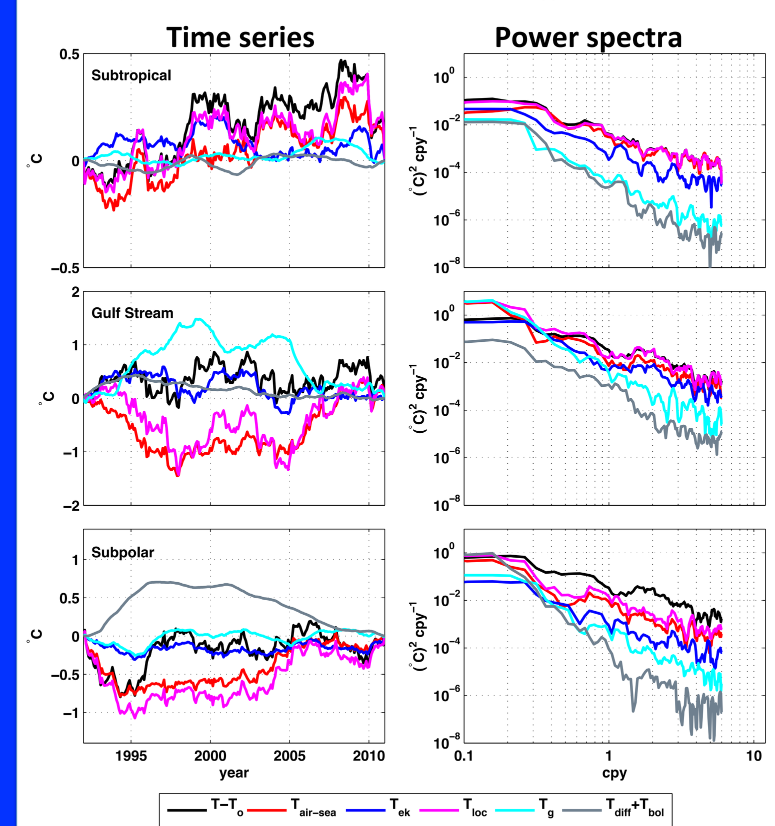

$$T_{ek} \equiv \int_0^t \frac{C_{ek}}{\rho_o C_p V}\, dt$$

$$T_g \equiv \int_0^t \frac{C_g}{\rho_o C_p V}\, dt$$

$$T_{loc} \equiv T_{air-sea} + T_{ek}$$

$$T_{bol} \equiv \int_0^t \frac{C_{bol}}{\rho_o C_p V}\, dt$$

1) Subtropical gyre
   - ➢ T_{loc} explains 91% of the variance of $T-T_o$
2) Gulf Stream
   - ➢ T_g important in $T-T_o$ budget
   - ➢ T_g and $T_{air-sea}$ anticorrelated (-0.90)
3) Subpolar gyre
   - ➢ T_{diff} and T_{bol} contribute to $T-T_o$ budget

(left panels) Time series and (right panels) power spectra for terms in (temporally integrated) T budget for (top) subtropical gyre (middle) Gulf Stream region and (bottom) subpolar gyre.

Conclusions

- Heat content integrated over the climatological mixed layer depth H is a useful measure of upper-ocean heat content.
- Both advection & air-sea heat fluxes play a role in variability in H_t, the tendency of H.
- Approximating the advective heat transport convergence as the sum of the Ekman & geostrophic convergences is successful over most of subtropical and subpolar gyres.
  - Exceptions: boundary regions of subpolar gyre, Mann Eddy region
- Over the interior of the subtropical and subpolar gyres >70% of the variance of H_t can be explained by local air-sea heat flux + Ekman transport variability.
- Geostrophic convergence plays a role along Gulf Stream Path.
- Importance of various terms in variance of H_t depends on timescale
  - Subtropical gyre: local forcing dominates on all timescales.
  - Gulf Stream: local forcing dominates for periods less than 6 months; geostrophic convergences increasingly important on longer timescales.
  - Subpolar gyre: local forcing dominates for periods less than 1 year; geostrophic transports, bolus transports, and diffusion play a role on longer timescales.
- Temporally integrated budgets emphasize terms important in H variability
  - Subtropical gyre: majority of H variance explained by local forcing
  - Gulf Stream region: geostrophic transports important, anti-correlated with air-sea heat fluxes ➔ H variability is forced by geostrophic convergences & damped by air-sea fluxes.
  - Subpolar gyre: diffusion and bolus transports also important

References

1. **Buckley, M.**, R. Ponte, G. Forget, and P. Heimbach. Low-frequency SST and upper-ocean heat content variability in the North Atlantic, subm. *J. Climate*.
2. Bjerknes, J., 1964. Atlantic air-sea interaction. *Advances in Geophysics*, **10**, 1-82.
3. Cayan, D. R., 1992. Latent and sensible heat flux anomalies over the northern oceans: Driving the sea surface temperature. *J. Phys. Oceanogr.*, **22**, 859–881.
4. Deser, C., M. A. Alexander, and M. S. Timlin, 2003. Understanding the persistence of sea surface temperature anomalies in midlatitudes. *J. Climate*, **16**, 57–72.
5. de Coetlogon, G. and C. Frankignoul, 2003: The persistence of winter sea surface temperature in the North Atlantic. *J. Climate*, **16**, 1364–1377
6. Frankignoul, C., P. Muller, and E. Zorita, 1997. A simple model of the decadal response of the ocean to stochastic wind forcing. *J. Phys. Oceanogr.*, **27**, 1533–1546
7. Kerr, R., 2000: A North Atlantic climate pacemaker for the centuries. *Science*, **288**, 1984–1986.
8. Knight, J. R., R. J. Allan, C. K. Folland, M. Vellinga, and M. E. Mann, 2005. A signature of persistent natural thermohaline circulation cycles in observed climate. *Geophys. Res. Lett.*, **32** (20).
9. Kushnir, Y., 1994. Interdecadal variations in North Atlantic sea surface temperatures and associated atmospheric conditions. *J. Climate*, **7**, 141-157.
10. Lozier, M.S., 2010. Deconstructing the conveyor belt. *Science*, **328**, 1507-1511.
11. Sturges, W., B.G. Hong, and A.J. Clarke, 1998, Decadal forcing of the North Atlantic subtropical gyre. *J. Phys. Oceanogr.*, **28**, 659-668.
12. Ting, Mingfang and Kushnir, Yochanan and Seager, Richard and Li, Cuihua. Forced and Internal Twentieth-Century SST Trends in the North Atlantic. *J. Climate*, **22**, 1469-1481.
13. Trenberth, K.E. and J.M. Caron, 2001: Estimates of meridional atmospheric and oceanic heat transports. *J. Climate*, **14**, 3433-3443.
14. Wunsch, C. and P. Heimbach, in press: Dynamically and kinematically consistent global ocean circulation and ice state estimates. Ocean circulation and climate: observing and modelling the global ocean, G. Siedler, J. Church, J. Gould, and S. Gries, Eds., Elsevier, 2d ed.
15. Wunsch, C., P. Heimbach, R. M. Ponte, and I. Fukumori, 2009: The global general circulation of the ocean estimated by the ECCO consortium. *Oceanography*, **22**, 88–103.